NANO LETTERS

2009
Vol. 9, No. 4
1636-1643

Fully Room-Temperature-Fabricated Nonvolatile Resistive Memory for Ultrafast and High-Density Memory Application

Yu Chao Yang,[†] Feng Pan,*[,†] Qi Liu,[‡] Ming Liu,[‡] and Fei Zeng[†]

Laboratory of Advanced Materials, Department of Materials Science and Engineering, Tsinghua University, Beijing 100084, People's Republic of China, and Laboratory of Nano-fabrication and Novel Devices Integrated Technology, Institute of Microelectronics, Chinese Academy of Sciences, Beijing 100029, People's Republic of China

Received January 1, 2009; Revised Manuscript Received February 16, 2009

ABSTRACT

Through a simple industrialized technique which was completely fulfilled at room temperature, we have developed a kind of promising nonvolatile resistive switching memory consisting of Ag/ZnO:Mn/Pt with ultrafast programming speed of 5 ns, an ultrahigh R_{OFF}/R_{ON} ratio of 10^7, long retention time of more than 10^7 s, good endurance, and high reliability at elevated temperatures. Furthermore, we have successfully captured clear visualization of nanoscale Ag bridges penetrating through the storage medium, which could account for the high conductivity in the ON-state device. A model concerning redox reaction mediated formation and rupture of Ag bridges is therefore suggested to explain the memory effect. The Ag/ZnO:Mn/Pt device represents an ultrafast and highly scalable (down to sub-100-nm range) memory element for developing next generation nonvolatile memories.

The semiconductor industry has long been seeking a high-density, high-speed, and low-power memory technology that retains its data even when the power is interrupted.[1] Though static random access memory (SRAM) and dynamic random access memory (DRAM) are very fast, both of them are volatile, which is a huge disadvantage, costing energy and additional periphery circuitry. Traditional nonvolatile flash memory based on charge storage is rapidly approaching its fundamental scaling limit due to the increasing difficulty of retaining electrons in shrinking dimensions. Moreover, it requires relatively long write time (>1 μs). Magnetic random access memory (MRAM) and ferroelectric random access memory (FRAM) also face severe problems in scaling. In this circumstance, a renewed nonvolatile memory concept called resistance-switching random access memory (RRAM), which is based on resistance change modulated by electrical stimulus, has recently inspired scientific and commercial interests due to its high operation speed, high scalability, and multibit storage potential.[1−3] The reading of resistance states is nondestructive, and the memory devices can be operated without transistors in every cell,[4,5] thus making a cross-bar structure feasible. A large variety of solid-state materials have been found to show these resistive switching characteristics, including solid electrolytes such as GeSe and Ag_2S,[5] perovskites such as $SrZrO_3$ and $Pr_{0.7}Ca_{0.3}MnO_3$,[3,6] binary transition metal oxides such as NiO, TiO_2, and ZnO,[7,8] and amorphous silicon (α-Si) as well as Si/α-Si core/shell nanowires.[2,9−11] Among them, binary transition metal oxides have simple compositions and exhibit resistive switching effects in polycrystalline states, in which case the requirements for deposition techniques, temperatures, and substrates are minimized. It is therefore of interest to investigate the possibility of fabricating a high-performance resistive memory based on binary transition metal oxides by conventional industrialized techniques at low temperatures, which holds potential for industrialization and three-dimensional (3D) stacking.

Here, we demonstrate the above-mentioned feasibility by developing a new kind of RRAM device consisting of Ag/ZnO:Mn/Pt with ultrafast programming speed of 5 ns, an ultrahigh R_{OFF}/R_{ON} ratio of 10^7, long retention time of more than 10^7 s, good endurance, and high reliability at elevated temperatures. The device preparation was completely accomplished by a simple magnetron sputtering method at

* Corresponding author, panf@mail.tsinghua.edu.cn.
[†] Laboratory of Advanced Materials, Department of Materials Science and Engineering, Tsinghua University.
[‡] Laboratory of Nano-fabrication and Novel Devices Integrated Technology, Institute of Microelectronics, Chinese Academy of Sciences.

10.1021/nl900006g CCC: $40.75
Published on Web 03/09/2009

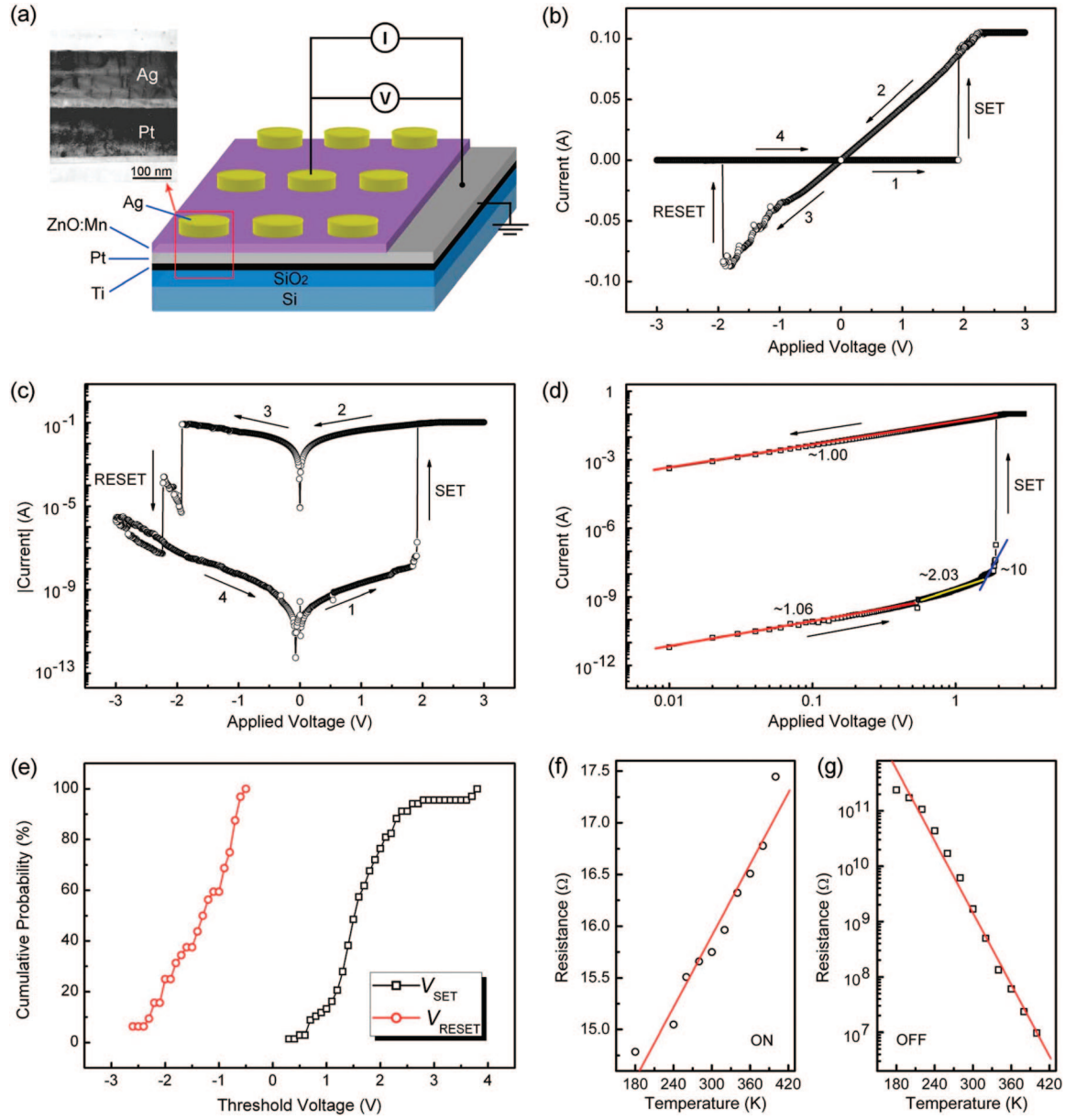

Figure 1. Resistance switching characteristics of the Ag/ZnO:Mn/Pt memory device. (a) A schematic configuration of the device. The inset shows a low-magnification cross section TEM image for the cell. $I-V$ curve of the Ag/ZnO:Mn/Pt device is shown in (b) linear scale, (c) semilogarithmic scale, and (d) log−log scale. (d) The linear fitting for the $I-V$ curve in log−log scale and the corresponding slopes for each portions. (e) The distributions of the threshold voltages of Ag/ZnO:Mn/Pt memory device. (f) Temperature dependence of R_{ON} of the device. R_{ON} decreases linearly with decreasing the ambient temperature, indicating that the bridges are in metallic states. (g) Temperature dependence of R_{OFF} of the device, implying a semiconducting character.

room temperature. Since these devices combine the advantage of flash with that of SRAM, they are very promising for future memory applications. Furthermore, we have successfully captured clear visualization of multiple metallic Ag bridges in ON-state devices via direct methods. A model concerning the formation and rupture of Ag bridges mediated by electrochemical redox reactions is therefore unambiguously suggested to account for the memory effect. The findings in this work imply a prospect of scaling the present device down to the sub-100-nm range and would have significance in understanding the resistive switching effects in RRAM devices.

A schematic configuration of the two-terminal devices studied in this work is depicted in Figure 1a. We adopted ZnO as the storage medium for its wide applications,[12] Ag as the top electrode (TE), and Pt as the bottom electrode (BE). The fabrication of the device was completely fulfilled by an industrialized magnetron sputtering method at room temperature (Supporting Information), thus holding intriguing promise for practical applications. Besides, 3% Mn dopants were introduced into ZnO aiming to enlarge the memory window via increasing the resistivity of the high resistance state (HRS), for Mn is a deep donor in ZnO and can significantly depress the concentration of intrinsic donors such as interstitial zincs or oxygen vacancies.[13,14] The as-grown ZnO:Mn film has a polycrystalline wurtzite structure with a weak *c*-axis orientation (Figure S1 in Supporting Information), and the manganese dopants exist in 2+ states

(Figure S2 in Supporting Information). A low-magnification transmission electron microscopy (TEM) image for the cross section of the cell is also shown in Figure 1a. As can be seen, the thicknesses of Ag TE, Pt BE, and the storage medium layer are about 90, 120, and 30 nm, respectively, while the lateral size of a bit cell is $\sim$300 μm.

The current−voltage ($I-V$) characteristics of the Ag/ZnO:Mn/Pt memory cell were studied by dc voltage sweep measurements to evaluate the memory effects of the obtained devices, and the results are illustrated both in linear (Figure 1b) and in semilogarithmic (Figure 1c) scales. During the measurements, the bias voltages were applied on the TE with the BE grounded, and neither a forming process nor a current compliance was necessary for activating the memory effect. The pristine device exhibits a high resistance $>10^9$ Ω, and the voltage was swept in a sequence of 0 V → 3 V → 0 V → −3 V → 0 V. By steady increase of the positive voltages imposed on the device, a pronounced change of resistance from the high resistance state (HRS or OFF) to the low resistance state (LRS or ON, $\sim$10−30 Ω) was observed at about 1.9 V, which is called the "SET" process. Subsequently, an opposite "RESET" process could also be seen when sweeping the voltage reversely to negative values, as evidenced by a two-step switching from LRS to HRS (Figure 1c). The first switching occurs at $\sim$−1.9 V, and the second switching takes place at $\sim$−2.2 V after the resistance of the cell stays in an intermediate state for a short while. The memory window defined by the two resistance states, i.e., $(R_{OFF} - R_{ON})/R_{ON} \approx R_{OFF}/R_{ON}$, is more than 10^7. This is an ultrahigh memory margin, making the periphery circuit very easy to distinguish the storage information ("1" or "0"). In addition, the write current of the device could be properly reduced, which will be shown afterward. The multistep RESET process is frequently observed in our devices, which might correspond to the ruptures of multifilaments with different threshold voltages (V_{th}). This phenomenon also implies a potential of multilevel data storage as long as an effective control for V_{th} could be realized. It is worthwhile to point out that the resistive switching behavior of our cell exhibits a typical bipolar nature, that is, the cell can only be written with a positive bias and erased with a negative one as verified by numerous measurements. Since filamentary rupture controlled by Joule heating shows no polarity dependence as in phase-change memories, thermal effects are not expected to play a dominant role in the RESET process of the present device even if they exist. The resistive switching effect in our case is very likely to be mediated by electrochemical redox reactions.[5]

To further understand the conduction and switching mechanisms of the memory device, the $I-V$ characteristics are replotted in a log−log scale. Figure 1d shows the logarithmic plot and linear fitting of the previous $I-V$ curve for the positive voltage sweep region, while it is similar for the negative branch. As shown in Figure 1d, the $I-V$ relationship in LRS clearly exhibits an Ohmic conduction behavior with a slope of 1.00, which is regarded to the formation of conductive filaments in the device during the SET process. However, the conduction mechanism in HRS is much more complicated. Fitting results for HRS show that the charge transport behavior is in good agreement with a classical trap-controlled space charge limited conduction (SCLC), which consists of three portions: the Ohmic region ($I \propto V$), the Child's law region ($I \propto V^2$), and the steep current increase region.[15] The totally different conduction behaviors in LRS and HRS also suggest that the high conductivity in ON-state device should be a confined, filamentary effect rather than a homogenously distributed one. This means that the active medium is in fact much smaller than the cell size, providing a potential of scaling.

Figure 1e shows the distributions of the switching threshold voltages (V_{SET} and V_{RESET}) of the device. When the Ag/ZnO:Mn/Pt memory was repeatedly switched between ON and OFF states, V_{RESET} distributes in a range of −2.6 to −0.5 V, while V_{SET} shows more scattering with a wider distribution of 0.3−3.8 V. The statistical analysis also yields the average values of V_{SET} and V_{RESET} as 1.6 and −1.3 V, respectively. Besides, it is reported that during a filament formation and rupture process, the formation of a filament (i.e., SET) should be more random than the destruction of an existing filament (i.e., RESET), since the formation process is determined by the competition among different filamentary paths.[16] Therefore one might expect larger variations in V_{SET} rather than in V_{RESET}, which is validated by many reports on such systems.[7,8,16] Since similar distributions are present in the Ag/ZnO:Mn/Pt memory, it might serve as another clue to the filamentary switching in our case.

As a key criterion for evaluating memory performance, fast programming speed is extremely desired for next generation nonvolatile memories. The programming speed of the Ag/ZnO:Mn/Pt devices was tested by applying pulse stimuli, and Figure 2c depicts a sequence of write/erase cycles stimulated by short pulses, namely, 3 V 5 ns bias (Figure 2a) for writing and −3 V 5 ns bias (Figure 2b) for erasing, respectively. The measurements were conducted after the as-prepared memory cell underwent a few switching cycles to get steady, and a small dc voltage of 0.1 V was used to read out the resistance states in the intervals of neighboring pulses. When a write pulse was applied on the device (see top panel of Figure 2c), a switching from OFF state to ON state was triggered with a large current as well as a low resistance recorded in the following read period (middle and bottom panels of Figure 2c). In contrast, an erase pulse switches the device back to OFF state. It is evident in Figure 2c that the switching process is reproducible from cycle to cycle, which confirms the feasibility of switching the present devices by 5 ns pulses. This programming speed has exceeded traditional DRAM, stood comparison with SRAM, and performed much better than other emerging memory technologies such as phase-change memories and molecular memories,[5,9,17,18] showing that our devices are robust for high-speed memory applications.

In order to depress the power consumption and enhance the overall stability of the memory elements, their write current should be properly reduced. Figure 2d displays the $I-V$ curve of the device with a lower write current of 5 mA. The resistance switching effects remain active under this

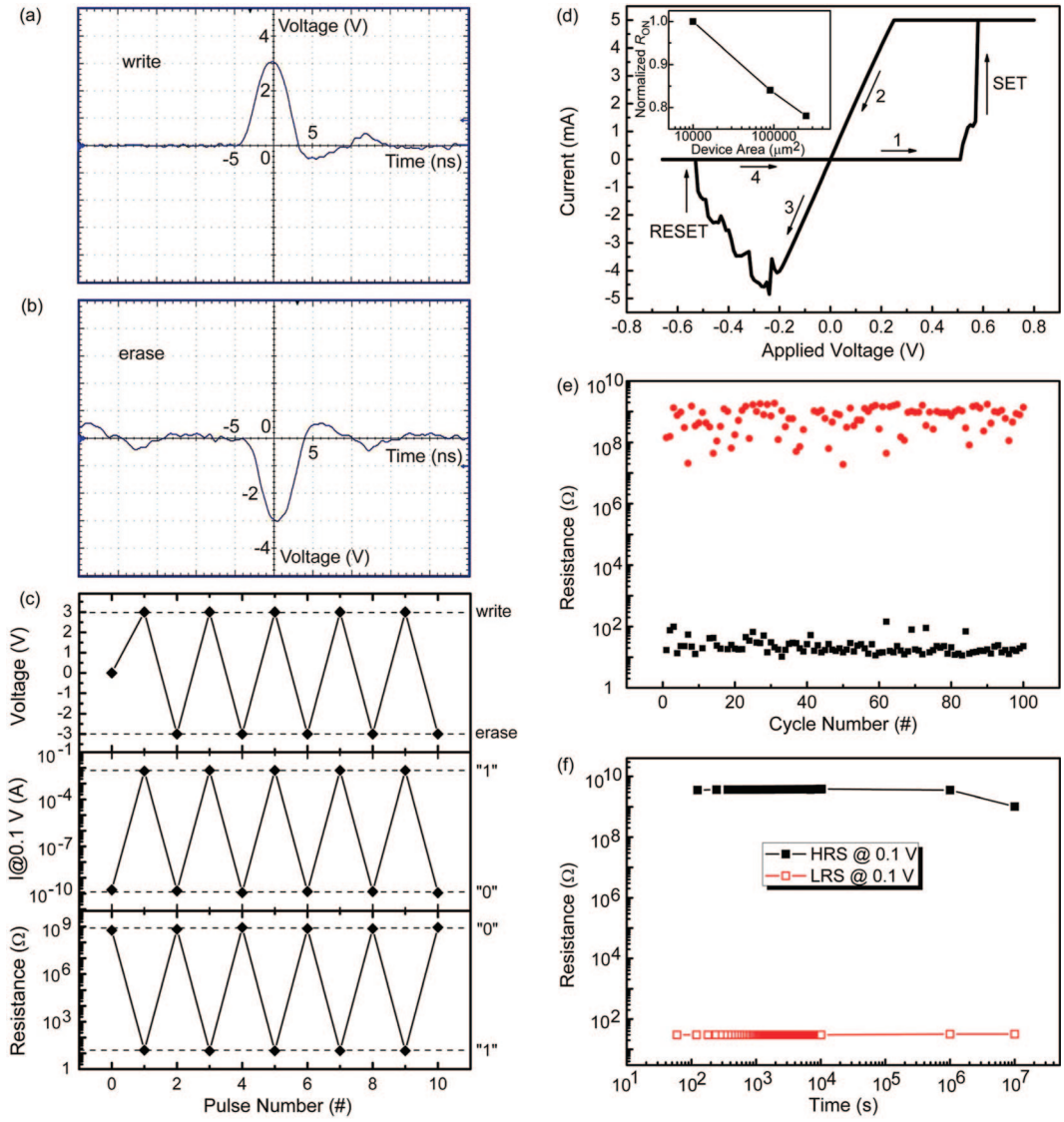

Figure 2. (a) The waveform of the write pulse. (b) The waveform of the erase pulse. (c) Write/erase cycles of the Ag/ZnO:Mn/Pt memory device utilizing short pulses. By applying a 3 V, 5 ns pulse for writing and a −3 V, 5 ns pulse for erasing, the memory device can be switched reproducibly between ON and OFF states. (d) $I-V$ curve of the device with a write current of 5 mA. The inset shows the dependence of normalized resistance in LRS on the device area. (e) Endurance performance of the Ag/ZnO:Mn/Pt device. (f) Retention of the Ag/ZnO:Mn/Pt memory in 10^7 s.

condition, while R_{ON} is increased to ~500 Ω at the same time, which is favorable for lowering the power dissipation. The R_{OFF}/R_{ON} ratio is still as large as 10^6 in this case. Figure 2e shows the endurance characteristics of the Ag/ZnO:Mn/Pt memory cell. The resistances of the two states scatter in a certain extent during cycling, especially for HRS. However, the extremely high R_{OFF}/R_{ON} ratio of the present device means tolerance to this kind of scatterings. As can be seen, the memory margin keeps beyond 10^5 during cycling, and the cell shows little degradation after 100 repeated sweep cycles. The endurance measurements ensured that the switching between ON and OFF states is highly controllable, reversible, and reproducible. After the device was switched ON or OFF, no electrical power was needed to maintain the resistance within a given state. The retention performance of the memory cell at room temperature is displayed in Figure 2f. One can see that the retention time of 10^7 s (~4 months) has been demonstrated for both of the two resistance states, while the information storage in this device is likely to persist for an even longer time judging from the present trend of data. Very recently, we noted that Lu and co-workers have developed a new temperature-accelerated algorithm to estimate the retention time of filamentary RRAM devices, in which way the long time for retention experiments could be spared.[10] We would try to study the device retention by this method in our following work.

Nowadays, the switching mechanisms in RRAM are still subjects of heated debate and controversy. The most plausible explanation is related to the filament formation and rupture. However, clear visualization of the conducting filaments in insulating oxides has been very challenging.[19] Moreover, there remain elusive questions in this kind of models, e.g., what is the microscopic nature of the filament, and whether a multiple filamentary model or a dominant filamentary model accord with the truth, etc. Answering the former question can lead to an understanding of the resistive

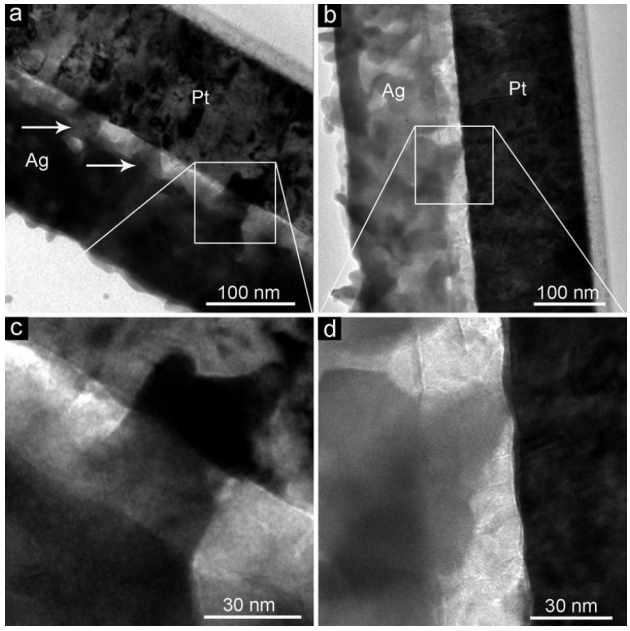

Figure 3. Conventional TEM observation for conductive filaments in the Ag/ZnO:Mn/Pt memory cell that has been switched ON. (a and b) Low-magnification cross section TEM images of the device. Both images show suspicious bridgelike regions with different shapes that might be identified as conductive paths, while multiple bridgelike regions could be observed in (a). (c and d) Enlarged images of the square regions in (a) and (b), respectively.

switching mechanism, while the latter one is of critical importance in development of high-density RRAM devices since it determines the performance stability during scaling. The above questions remain elusive mainly because the filaments were rarely observed and thus hardly analyzed comprehensively. The observations for conducting paths were most frequently reported in conductive atomic force microscopy (CAFM) characterizations.[20−22] Though a powerful tool is CAFM, the microscopic nature of the filaments such as the composition as well as the chemical state are not easy to be clarified by this method. Besides, there are a few other attempts to unveil the nature of the filaments. Guo et al. have reproduced and inspected filament formation in a $Pt/H_2O/Ag$ model system to simulate the situation in solid electrolytes.[23] Sakamoto et al. directly observed a single Cu protrusion in solid electrolytes via TEM observations, whereas a complete formation of bridge was not demonstrated in their case, since the connection between the protrusion and TE was invisible.[24] Moreover, even if it was seen, more convincing methods are required to examine the solid formation of bridges before drawing a conclusion. Aiming at disclosing the characters of the so-called "filament" better, we have tried to seek for conductive paths in Ag/ZnO:Mn/Pt memory devices under TEM, and panels a and b of Figure 3 show cross section TEM images of the memory cell which has been switched ON. One can see several suspicious dark regions as marked by squares and arrows therein. Panels c and d of Figure 3 show enlarged images of the square regions in panels a and b of Figure 3, respectively. One can clearly observe that the protrusion-like regions have connected the TE and BE thoroughly, and bridges are consequently built. The protrusions in Figure 3a are nearly cylindrical, while that in Figure 3b shows an inclined conical shape. The typical size of the bridges is 30−50 nm. It should be noted that all these protrusions shown in Figure 3 exist in an identical memory cell, which effectively underpins a multifilament switching. However, single-filament switching has also been claimed by either scaling the device down to nanoscale[10] or employing a limited programming current,[21] and Szot and colleagues have proved that single dislocations in $SrTiO_3$ may serve as substantial memory elements by individually addressing them and observing clear bistable resistance switching.[20] As an attempt to verify the interrelation between the two types of switching, the device area dependence of normalized R_{ON} of Ag/ZnO:Mn/Pt memory is plotted in the inset of Figure 2d. When the device area is reduced by 96%, the R_{ON} of the device increases ~22%. This observation is consistent with some other reports,[9,25] which might indicate that the number of the filaments would scale with the cell size. Therefore, it is reasonable to expect a transition from multifilament switching to single-filament switching if scaling the device down to nanoscale. It is most probable that both types of switching can occur depending on the conditions such as the cell size as well as the programming current.

To determine the nature of the bridgelike regions, the samples were further delivered to analytical TEM. Figure 4 shows a *Z*-contrast image of the bridgelike region displayed in Figure 3c and the high-resolution energy dispersive X-ray spectroscopy (EDX) analysis results for representative areas. It is well-known that the contrast in *Z*-contrast images reflects an ability of elastically scattering electrons, which is approximately proportional to Z^2 (Z represents the atomic number of the element). One can see that the bridge is bright in Figure 4, similar with the Ag TE and Pt BE, which indicates that it is composed of elements with high atomic numbers. Furthermore, EDX analysis was performed in scanning transmission electron microscopy (STEM) mode. The adopted convergent electron beam in this mode has a diameter of 0.8 nm, which is smaller than the parallel beam used in conventional TEM mode. With the aid of this local method, one can study the compositions of specific interesting regions with high space resolution. The EDX spectrum collected in the storage medium apart from the bridge is displayed in Figure 4a, which resembles that collected from the ZnO:Mn layer of the OFF-state device in conventional TEM mode (Figure S3 in Supporting Information). One can see in Figure 4a that three concerned elements including Zn, Mn, and O were detected, confirming a pure ZnO:Mn phase. The unexpected Cu and Si contaminations are regarded to be introduced from the TEM grid and the substrates in the process of ion-beam thinning, respectively. In contrast, the EDX spectrum taken from the body of the bridge exhibits very strong Ag peaks with weakened signals of ZnO:Mn (Figure 4b). This distinct difference implies the fact that the bridge might be formed via Ag percolation in ZnO matrix. Figure 4c shows the EDX spectrum collected from the interface between the bridge and Pt BE. Besides the signals coming from Pt, strong Ag peaks are still visible in this case,

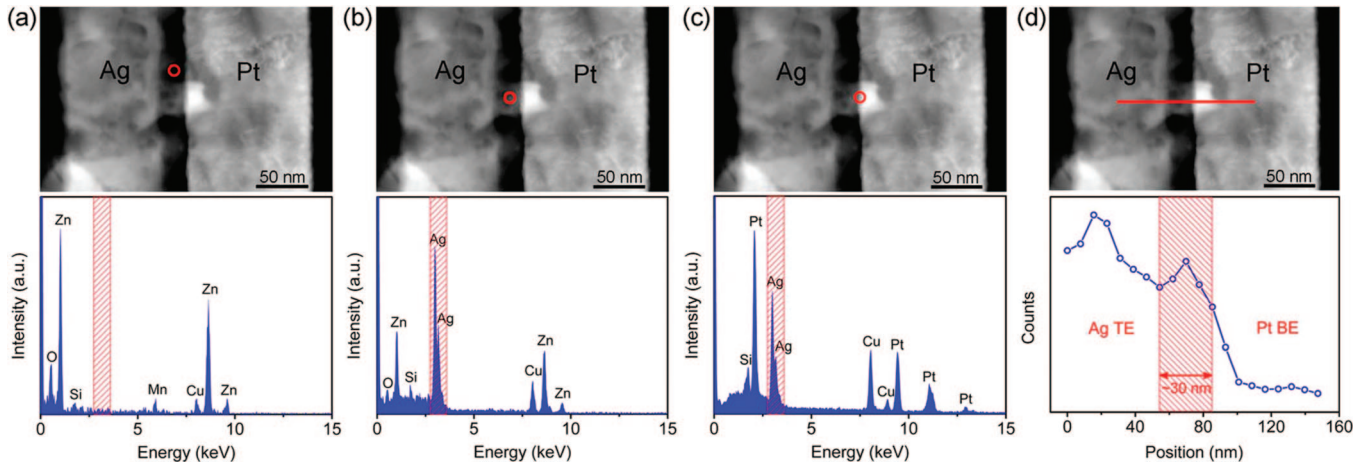

Figure 4. *Z*-contrast image and high-resolution EDX analysis in STEM mode for the bridgelike region in ON-state device. The top panels of (a), (b), (c), and (d) show cross section *Z*-contrast image of the device, in which the regions for EDX analyses were correspondingly marked. (a) EDX spectrum collected in the storage medium apart from the bridge, indicating a pure ZnO:Mn phase. (b) EDX spectrum collected from the body of the bridge; therein a strong Ag signal was detected. (c) EDX spectrum collected from the protrusion/Pt interface, revealing that Ag has extended to the BE and forms a complete bridge. (d) A line profile concerning the intensity of Ag along the bridge. The results show that the protrusions composed of Ag have not only connected the electrode pair completely but extended into Pt BE.

demonstrating that Ag has already extended to the BE and forms a complete pathway between the electrode pair. To verify the above suppositions, a line profile concerning the intensity of Ag signals along the bridge has been surveyed (Figure 4d). The intervals between adjacent spots were ~8 nm, and the counts of each spot in the line profile reflect the integral of the region as marked by shadows in Figure 4a−c. It is apparent in Figure 4d that the quantity of Ag keeps at a high level until the Pt BE is reached, which is rational only if the bridge is composed of Ag. Moreover, a moderate intensity of Ag is still detectable at ~8 nm underneath the bridge/Pt interface. The result implies that the Ag protrusion has not only penetrated through the ZnO:Mn layer thoroughly but extended into Pt BE. Analyses for other bridgelike regions in Figure 3 have brought us to the same conclusions.

Therefore, via TEM and *Z*-contrast image observations as well as high-resolution EDX analysis, we have successfully clarified three issues: (i) bridgelike regions were directly observed under TEM, validating the hypothesis that the high conductivity in LRS is a filamentary effect; (ii) multiple bridges exist in one identical Ag/ZnO:Mn/Pt memory device, which implies that the write current would scale with the cell size, thus avoiding the possible heat concerns and overall instability during scaling;[25] and (iii) the bridges are mainly composed of Ag element. Here, one new question naturally arises: what kind of chemical state does Ag exist as in these conductive bridges? We will resolve this issue thereinafter.

Parts f and g of Figure 1 show the temperature dependence of R_{ON} and R_{OFF} of the device, respectively, and the measurements were carried out in a vacuum environment. As shown in Figure 1f, R_{ON} exhibits a decreasing trend when the ambient temperature decreases. This is a typical electronic transport behavior for a metal, in which phonon scattering is dominant. The temperature dependence of metallic resistance can be written as $R(T) = R_0[1 + a(T - T_0)]$, where R_0 is the resistance at temperature T_0, and α is the temperature coefficient of resistance.[26] Our fitting results for $R_{ON}-T$ comply with this linear dependence (see Figure 1f); therefore the bridges observed above are deemed to be composed of Ag in metallic states. This judgment is also supported by the linear $I-V$ characteristics of LRS as shown in parts b and d of Figure 1. By choosing T_0 as 300 K, the α of the bridges is further calculated to be 7.3×10^{-4} K^{-1}, which is smaller than the value $\sim 4 \times 10^{-3}$ K^{-1} reported in defect-free Ag nanowires with a similar size of 30 nm in diameter.[27] This discrepancy is attributed to inevitable defects in the Ag bridges, since the presence of defects can significantly reduce the value α by shortening the mean free path of electrons.[27] On the other hand, Figure 1g shows that R_{OFF} increases with decreasing temperature, and it exhibits an approximate relationship $\log R_{OFF} \propto T$, which could be ascribed to a typical semiconducting behavior. The temperature dependence of current in a semiconductor follows

$$I = I_0 \exp(-\phi_t/\kappa T)$$

where κ is the Boltzmann constant and ϕ_t is the thermal activation energy. By employing an Arrhenius plot, the ϕ_t of the system was calculated to be ~490 meV in the temperature regime 260−400 K (Figure S4 in Supporting Information). This large ϕ_t may be due to deep donor states introduced by Mn doping.[13,14] Moreover, it should be noted that the R_{OFF}/R_{ON} ratio remains 10^5-10^6 at 400 K, demonstrating good memory reliability at elevated temperatures. This character endows the memory device with tolerance to a heated environment.

By combination of the bipolar resistive switching character with the presence of metallic Ag bridges, a clear picture for the resistive switching effects in Ag/ZnO:Mn/Pt memory cell has emerged gradually, namely, a redox-controlled Ag bridge creation and rupture process. Figure 5 illustrates a schematic diagram for the switching mechanism: when a positive voltage is applied to Ag TE, oxidation occurs on this electrochemically active material. Therefore Ag^+ cations are generated, which could be described as $Ag \rightarrow Ag^+ + e^-$ (Figure 5a). The mobile Ag^+ cations migrate toward Pt BE

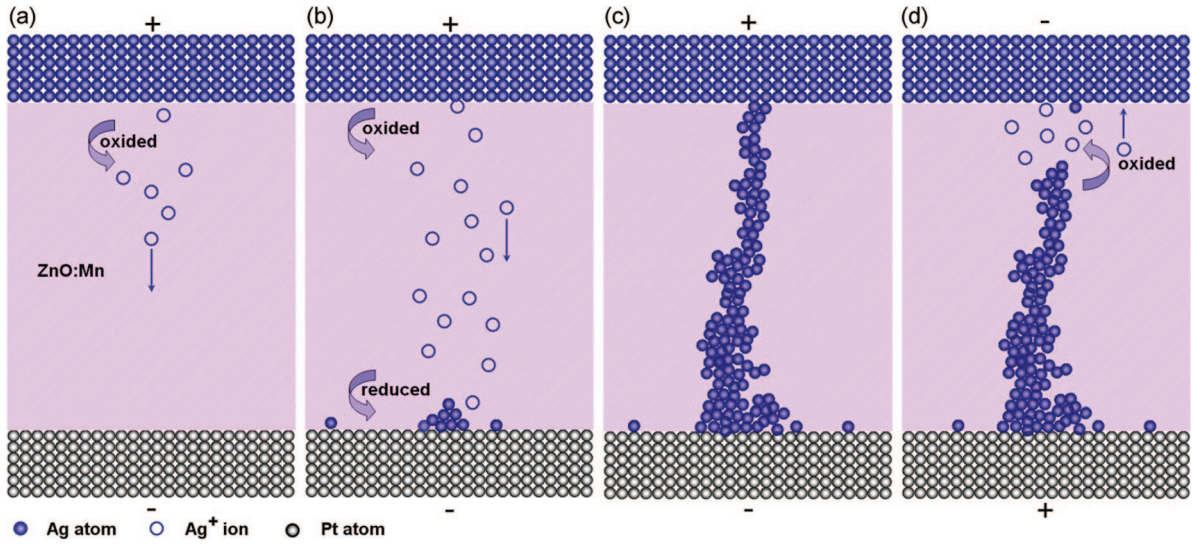

Figure 5. A schematic diagram for the mechanism of resistive switching effects in Ag/ZnO:Mn/Pt devices. (a) The oxidation of Ag at TE. (b) The migration of the mobile Ag^+ cations toward the cathode and their reductions therein. (c) The precipitations of Ag metal atoms at the Pt electrode lead to a growth of Ag protrusion and finally form a highly conductive bridge in the cell. (d) When the polarity of the applied voltage is reversed, an electrochemical dissolution of the bridge takes place, resetting the system into the OFF state.

through the ZnO:Mn layer and are reduced there by electrons flowing from the cathode, i.e., $Ag^+ + e^- \rightarrow Ag$ (Figure 5b). The successive precipitations of Ag metal atoms at the cathode lead to a growth of the Ag protrusion, which finally reaches the TE and forms a highly conductive path in the ON state (Figure 5c). When the polarity of the applied voltage is reversed, an electrochemical dissolution takes place somewhere along the bridge, resetting the system into the OFF state (Figure 5d). Although where the rupture is carried out is still unclear in this field, it is usually suggested to occur in the weakest part of the bridge.[23] Joule heating effects were not taken into account in the switching process for their subordinate importance in this case. It is conceivable that the formation of the Ag bridges would inevitably impose influence on the crystalline structure of the ZnO:Mn layer, which actually manifests itself as deteriorating the structure of ZnO:Mn from a *c*-axis oriented polycrystalline wurtzite to a more disordered polycrystalline wurtzite structure. This transformation has been reflected by the evolution of selected area electron diffraction (SAED) patterns from some discrete diffraction arcs in as-grown film to a series of diffraction rings in ON-state device (Figure S5 in Supporting Information), which thereby corroborates our explanation for the switching mechanism.

The present Ag/ZnO:Mn/Pt memory device provides a good candidate for next generation nonvolatile memories. First, it is exceptionally fast, thus combining the advantage of SRAM with that of flash. The programming speed of 5 ns is fastest among emerging nonvolatile memory concepts to date, while the switching time in this type of memory could be further reduced by increasing the applied voltage.[5] Second, the memory margin defined by the R_{OFF}/R_{ON} ratio is more than 10^7, which minimizes the efforts of a periphery circuit to distinguish the storage information. Moreover, it possesses robust endurance, long retention, and good reliability at elevated temperatures. Last but not least, it holds huge potential for miniaturization and industrialization. The typical size of the Ag filaments observed in this work is several tens of nanometers, which provides a prospect of scaling the present device down to the sub-100-nm range. Suppose that the devices were scaled to 50 nm and they were organized in a planar cross-bar structure (cell size, $4F^2$, F denotes feature size used for patterning the cell), a packing density of 10 gigabit cm^{-2} would be realized. Moreover, the full room-temperature fabrication offers the memory a feasibility of stacking in 3D mode;[4,28] thus the cell size might be further scaled down to $(4/n)F^2$ (where n is the memory layer number in 3D stack) and result in much higher density such as 1 terabit cm^{-2}. One should specially note that all the good characteristics of the devices were obtained via an industrialized fabrication method. An ultimate replacement for flash and DRAM by this type of memory is not out of reach.

In summary, we have developed a kind of fully room-temperature-fabricated Ag/ZnO:Mn/Pt RRAM device with robust performance. A model concerning the formation and rupture of Ag bridges mediated by redox reactions is suggested to account for the memory effect based on concrete observations of metallic Ag bridges. The situation reported in this work is not necessarily limited to the present case of Ag/ZnO:Mn/Pt but may also apply to a wide range of RRAM devices. Beyond mere memory applications, the Ag/ZnO:Mn/Pt cells are also promising for nonvolatile switches in reconfigurable large-scale integrated circuits (LSIs).[24] Improvement of the memory device would be focused on further scaling the device size and reducing the write current.

Acknowledgment. We thank D. P. Yu and J. M. Zhang for TEM, STEM, and EDX analyses, and we thank R. Jia for varied temperature experiments. This work was supported by National Hi-tech (R&D) project of China (Grant

No.2006AA03Z435) and National Natural Science foundation of China (Grant No. 50772055, 50871060).

Supporting Information Available: Cross section TEM characterization of the as-grown ZnO:Mn film, XPS analysis, EDX spectrum collected from the ZnO:Mn layer of the OFF-state device in conventional TEM mode, Arrhenius plot for the current−temperature curve yielding ϕ_t of the system, and SAED pattern evolution of ZnO:Mn layer during the SET process. This material is available free of charge via the Internet at http://pubs.acs.org.

References

(1) Meijer, G. I. *Science* **2008**, *319*, 1625–1626.
(2) (a) Dong, Y.; Yu, G.; McAlpine, M. C.; Lu, W.; Lieber, C. M. *Nano Lett.* **2008**, *8*, 386–391. (b) Lu, W.; Lieber, C. M. *Nat. Mater.* **2007**, *6*, 841–850.
(3) Beck, A.; Bednorz, J. G.; Gerber, Ch.; Rossel, C.; Widmer, D. *Appl. Phys. Lett.* **2000**, *77*, 139–141.
(4) Lee, M.-J.; Park, Y.; Suh, D.-S.; Lee, E.-H.; Seo, S.; Kim, D.-C.; Jung, R.; Kang, B.-S.; Ahn, S.-E.; Lee, C. B.; Seo, D. H.; Cha, Y.-K.; Yoo, I.-K.; Kim, J.-S.; Park, B. H. *Adv. Mater.* **2007**, *19*, 3919–3923.
(5) Waser, R.; Aono, M. *Nat. Mater.* **2007**, *6*, 833–840.
(6) Liu, S. Q.; Wu, N. J.; Ignatiev, A. *Appl. Phys. Lett.* **2000**, *76*, 2749–2751.
(7) (a) Choi, B. J.; Jeong, D. S.; Kim, S. K.; Rohde, C.; Choi, S.; Oh, J. H.; Kim, H. J.; Hwang, C. S.; Szot, K.; Waser, R.; Reichenberg, B.; Tiedke, S. *J. Appl. Phys.* **2005**, *98*, 033715. (b) Baek, I. G.; Lee, M. S.; Seo, S.; Lee, M. J.; Seo, D. H.; Suh, D.-S.; Park, J. C.; Park, S. O.; Kim, H. S.; Yoo, I. K.; Chung, U.-In.; Moon, J. T. *IEDM Tech. Dig.* **2004**, 587–590.
(8) (a) Xu, N.; Liu, L. F.; Sun, X.; Liu, X. Y.; Han, D. D.; Wang, Y.; Han, R. Q.; Kang, J. F.; Yu, B. *Appl. Phys. Lett.* **2008**, *92*, 232112. (b) Chang, W. Y.; Lai, Y. C.; Wu, T. B.; Wang, S. F.; Chen, F.; Tsai, M. J. *Appl. Phys. Lett.* **2008**, *92*, 022110.
(9) Jo, S. H.; Lu, W. *Nano Lett.* **2008**, *8*, 392–397.
(10) Jo, S. H.; Kim, K.-H.; Lu, W. *Nano Lett.* **2009**, *9*, 496–500.
(11) Jo, S. H.; Kim, K.-H.; Lu, W. *Nano Lett.* **2009**, *9*, 870–874.
(12) Pan, F.; Song, C.; Liu, X. J.; Yang, Y. C.; Zeng, F. *Mater. Sci. Eng. R.* **2008**, *62*, 1–35.
(13) Han, J.; Senos, A. M. R.; Mantas, P. Q. *J. Eur. Ceram. Soc.* **2002**, *22*, 1653–1660.
(14) Shinde, V. R.; Gujar, T. P.; Lokhande, C. D.; Mane, R. S.; Han, S.-H. *Mater. Chem. Phys.* **2006**, *96*, 326–330.
(15) Lampert, A.; Mark, P. *Current Injection in Solids*; Academic: New York, 1970.
(16) Wang, Z.; Griffin, P. B.; McVittie, J.; Wong, S.; McIntyre, P. C.; Nishi, Y. *IEEE Electron Device Lett.* **2007**, *28*, 14–16.
(17) Brewer, J. E.; Zhirnov, V. V.; Hutchby, J. A. *IEEE Circuits Devices Mag.* **2005**, *21*, 13–20.
(18) Muller, G.; Happ, T.; Kund, M.; Lee, G. Y.; Nagel, N.; Sezi, R. *IEDM Tech. Dig.* **2004**, 567–570.
(19) Sawa, A. *Mater. Today* **2008**, *11*, 28–36.
(20) Szot, K.; Speier, W.; Bihlmayer, G.; Waser, R. *Nat. Mater.* **2006**, *5*, 312–320.
(21) Schindler, C.; Szot, K.; Karthäuser, S.; Waser, R. *Phys. Status Solidi RRL* **2008**, *2*, 129–131.
(22) Yun, J.-B.; Kim, S.; Seo, S.; Lee, M.-J.; Kim, D.-C.; Ahn, S.-E.; Park, Y.; Kim, J.; Shin, H. *Phys. Status Solidi RRL* **2007**, *1*, 280–282.
(23) Guo, X.; Schindler, C.; Menzel, S.; Waser, R. *Appl. Phys. Lett.* **2007**, *91*, 133513.
(24) Sakamoto, T.; Lister, K.; Banno, N.; Hasegawa, T.; Terabe, K.; Aono, M. *Appl. Phys. Lett.* **2007**, *91*, 092110.
(25) Ahn, S.-E.; Lee, M.-J.; Park, Y.; Kang, B. S.; Lee, C. B.; Kim, K. H.; Seo, S.; Suh, D.-S.; Kim, D.-C.; Hur, J.; Xianyu, W.; Stefanovich, G.; Yin, H.; Yoo, I.-K.; Lee, J.-H.; Park, J.-B.; Baek, I.-G.; Park, B. H. *Adv. Mater.* **2008**, *20*, 924–928.
(26) Guan, W.; Liu, M.; Long, S.; Liu, Q.; Wang, W. *Appl. Phys. Lett.* **2008**, *93*, 223506.
(27) Bid, A.; Bora, A.; Raychaudhuri, A. K. *Phys. Rev. B* **2006**, *74*, 035426.
(28) Lee, M.-J.; Kim, S. I.; Lee, C. B.; Yin, H.; Ahn, S.-E.; Kang, B. S.; Kim, K. H.; Park, J. C.; Kim, C. J.; Song, I.; Kim, S. W.; Stefanovich, G.; Lee, J. H.; Chung, S. J.; Kim, Y. H.; Park, Y. *Adv. Funct. Mater.* **2008**, *18*, 1–7.

NL900006G